Seismo Electromagnetics: Lithosphere-Atmosphere-Ionosphere Coupling, Eds. M. Hayakawa and O.A. Molchanov, pp 117-130

A physical model of Electric Earthquake Precursors due to crack propagation and the motion of charged edge dislocations

Andreas Tzanis[1] and Filippos Vallianatos[2]

[1] *Department of Geophysics and Geothermy, University of Athens, Panepistimiopoli, Zografou 15784, Greece*
[2] *Technological Educational Institute of Crete, Chania Branch, 3 Romanou St., Chania 73133, Crete, Greece.*

We present a model of spontaneous electric current generation (electrification) involving the motion of charged edge dislocation arrays, during crack formation and propagation (microfracturing) in rocks under stress. Inasmuch as the seismogenic zone comprises a rock volume filled with cracks, massive pre-seismic crack propagation may produce macroscopic electrical earthquake precursors by the superposition of the electric fields of propagating cracks, varying proportionally to the changes in dislocation /crack density and rock resistivity. The motion of dislocations occurs parallel to the applied shear stress, generating a dipole electric field parallel to their slip vector, hence quasi-parallel to the slip vector of shear cracks and by the self-similarity of fragmentation processes, to the slip vector of the upcoming earthquake. We simulate the evolution of crack populations using an *ad hoc* kinetic theory based on Maxwell-Boltzman statistics. Our results indicate that crack propagation evolves according to a limited class of time functions with characteristic bay and bell-like shapes. This allows for the generation of a limited class of electric precursors with analogous shape and duration varying from a few tens of seconds to a few hours. Massive crack propagation is only expected to appear at the last several hours to several days prior to rupture, defining the scale of the time lag between the precursor and the earthquake. Finally, we investigate the effect of the self-similar geometry of brittle failure, on the signal. We derive, from first principles, a self-similar scaling law relating the amplitude of the observed precursor with the magnitude of the earthquake with an expression of the form $\log\mathbf{E}=C_s+\alpha M$, with $\alpha\approx 0.35$. The slope is universal under the conditions for which it has been derived, but C_s depends on the source properties and the source-receiver path. The model has been applied to the analysis of electric signals reported to have preceded large earthquakes in the area of Greece, and successfully reproduced their temporal and spatial characteristics. Emphasis in given to the fact that the spatial characteristics of the observed signals could be reproduced with buried electric dipole configurations closely related to the focal mechanism solutions of the respective earthquakes.

1. Introduction

Microfracturing electrification, i.e. the appearance of spontaneous charge production and transient electric and electromagnetic emission (E-EME) associated with the opening and propagation of microcracks, has been discussed by several authors in connection to laboratory experiments (e.g. Warwick et al., 1982; Ogawa et al., 1985; Cress et al., 1987; Enomoto and Hashimoto, 1990). Warwick et al. (1982), have measured current spikes from individual microcracks of the order 10^{-3} A, associated with crack opening times of the order of 10^{-6} s, thus providing a net charge density of 10^{-3} C/m^2 using $q\approx it/l^2$ where $l\approx 10^{-3}$m is the order of the crack length. A similar value of 10^{-2} C/m^2 is reported by Ogawa, et al. (1985), while Enomoto and Hashimoto (1990) measured a charge production of 10^{-9} C for cracks with surface of the order 10^{-6} m^2, yielding a charge density of 10^{-3} C/m^2. More recent experiments observe simultaneous E-EME and acoustic emissions (AE) from opening microcracks in both piezoelectric and non-piezoelectric materials (Fiffolt et al., 1993; Enomoto et al., 1994; Hadjicontis and Mavromatou 1994, 1996; Chen et al., 1994; Yoshida et al., 1994; Yoshida et al., 1997). In all cases, the intensity of microfracturing and E-EME accelerated shortly prior to failure and the electric field amplitudes were of the order of V/m, associated with currents of the order of nA/cm^2. With the exception of Chen et al. (1994), E-EME was observed only in dry rock specimens.

Piezoelectricity has been shown to electrify quartz-bearing rocks (e.g. Nitsan, 1977; Warwick et al., 1982; Yoshida et al., 1997). Additional mechanisms have also been considered for non-piezoelectric materials, including contact or separation electrification, (Ogawa et al., 1985), the motion of charged edge dislocations, (Slifkin, 1993; Hadjicontis and Mavromatou, 1996; Ernst et al., 1993; Vallianatos and Tzanis 1998, 1999a) and the ionisation of the void space within the crack and acceleration of unbounded electrons (Cress et al., 1987). Freund and Borucki (1999) demonstrate the existence of positive-hole dormant charge carriers in quartz-free or low-quartz rocks, that can be activated by low velocity impacts, and suggest that similar activation may take place by acoustic waves or direct impulses during crack propagation. Finally, in a very interesting experiment, Bella et al., (1994) observe simultaneous AE and EME under field conditions in caves, which they attribute to pressure variations inducing frictional sliding and charge separation between adjacent rock blocks. It is apparent that microfracturing electrification involves a multitude of phenomena whose relative contribution cannot be determined because they may be operative or inoperative and synergistic or competitive in a complex and poorly understood manner, depending on the material and its past mechanical and thermal history, as well as its present state. Theoretical work to this effect is still infant (e.g. Teisseyre and Nagahama, 1999). Note however that of all the mechanisms quoted above, one is *always* present during brittle fracture: *the motion of charged edge dislocations (MCD)*, which we will examine herein.

Whitworth (1975) provides a thorough background of charged edge dislocations. MCD is thought to electrify a crystalline structure in two ways. At normal temperatures, sudden stress changes below a certain threshold do not produce dislocation motion with macroscopic plastic yielding, because of substantial stress barriers and the pinning of dislocations due to elastic and coulombic interactions with other defects (e.g. Slifkin, 1993). There can, however, be a displacement (bowing out) of the free dislocation core segments between the pinning points, which cannot be compensated for by the slowly diffusing (10^0-10^6s at temperatures < 400°C) space charge cloud surrounding the dislocation core. This leaves a long-lived separation of the dislocation core from the centre of mass of the space charge distribution and produces an electric dipole with dipole moment of the order 10^{-19} C-m/m, oriented in the slip plane and perpendicular to the dislocation line. Under such conditions there's no internal stress change and any external stress pulse would propagate very fast through the earth, (in a matter of seconds over kilometric scale distances), so that only short duration transients could be generated by such a mechanism.

In order to account for longer lasting pre-seismic electric variations, in the present paper we consider the case of non-elastic deformation, when the stress exceeds a critical level and dislocations begin to multiply, break away from their pinning points and migrate through the lattice expanding to new loops between stronger pinning points. If an obstacle occurs, the moving dislocations will pile up against it, concentrating stress and initiating a crack at the head of the pileup. Since the time constants of crack opening are of the order 10^{-3}-10^{-7}s, (for opening velocities of the order 10^3m/s), any longer lasting response of the space charge cloud will result in an elongated electric dipole, again in the slip plane and perpendicular to the dislocation line. It also appears reasonable to suggest that moving dislocations, acting as stress concentrators, may guide and focus additional effects. For instance they may propel dormant charge carriers; bond breaking and separation effects take place in their slip plane, while bound charges are released due to piezoelectric polarisation reduction resulting from the stress drop caused by crack opening (as in Yoshida et al., 1997). Determining how these multiple mechanisms interact and may be a prized objective, but will not concern us here. We assume that the additional effects are integrated in the microfracturing / MCD process.

Attempts to associate microfracturing / MCD electrification and non-elastic deformation have been made by Ernst et al. (1993), Nomikos and Vallianatos (1997) and Vallianatos and Tzanis (1998, 1999a). Herein, we attempt a discussion of microfracturing / MCD electrification during large scale crack propagation, simulate the time dependence of the process and hence, the characteristics of the precursory transient electric signal (if any), faraway from the source. Eventually, we construct a physical model of transient electrical earthquake precursors (EEP), which we apply to the examination and interpretation of physical signals recorded prior to large earthquakes in Greece.

2. Electrification by the microfracturing/MCD mechanism

Dislocations may occur in different mechanical 'flavours', which would move in opposite directions. Thus, although the dislocation density may be as high as 10^{14}/m^2 for heavily deformed materials and both flavours carry comparable charges, any net electrical polarisation of one sign must be the result of a net excess of charged dislocations with a particular mechanical flavour. Such an excess may have been introduced into crustal rocks, in order to accommodate previous cycles of non-elastic deformation and bending or folding (also see Slifkin, 1993 for an example). Vallianatos and Tzanis (1998, 1999a) show that the MCD current density is

$$J = \sqrt{2} \cdot \frac{\Lambda^+ - \Lambda^-}{\Lambda^+ + \Lambda^-} \cdot \frac{q_l}{\mathbf{b}} \cdot \frac{\partial \varepsilon}{\partial t} = C \cdot \delta\Lambda \cdot q_l \cdot \dot{\varepsilon} \qquad (1)$$

where Λ^+ and Λ^- are the dislocation densities of opposite flavours, $\delta\Lambda$ the excess dislocation density, q_l is the charge per unit length on the dislocation (of the order 10^{-11} Cb/m), and $\varepsilon = ½(\Lambda^+ + \Lambda^-)\cdot\mathbf{b}\cdot\delta x$ is the plastic contribution to strain, when edge dislocations of Burgers vector **b** move through a distance δx. J is related with the MCD density and velocity vector via a generalisation of Orowan's law ($\dot{\varepsilon} \approx \Lambda\upsilon$). Eq. (1) shows that the observed transient electric variation is related to the non-stationary accumulation of deformation in the neighbourhood of the moving dislocations. Interestingly enough, the ratio $(\Lambda^+ + \Lambda^-)/(\Lambda^+ - \Lambda^-)$ is usually between 1 and 1.5 in alkali halides (Whitworth, 1975). Assuming the highest value for rocks, i.e. lower excess dislocation density, and $\partial\varepsilon/\partial t \approx 10^{-4}$ s^{-1}, approx. equal to co-seismic deformation rates, we obtain $J \approx 5\times10^{-6}$ A/m^2 $\approx$ 0. 5 nA/cm^2, which is comparable to the values quoted from the international experimental literature.

Next, consider that the motion of dislocation arrays may result in crack formation by the piling-up of the linear defects when the leading dislocation(s) get locked by some obstacle. The stress concentration near the first locked dislocation of an array is equivalent to the product of the applied stress times the number of dislocations in the array (Eshelby et al., 1951). Propagation of cracks occurs when a new dislocation array enters into the crack. The dislocation-to-crack process has been considered by Stroh (1954), for interactions along a single dislocation plane, on which dislocations move under the influence of an external stress field. Figure 1a illustrates a tensile (Mode I) crack forming by ν edge dislocations moving on a plane perpendicular to the paper. The maximum tensile stress occurs at the tip of the array and at an angle $\theta \approx 70.5°$, (e.g. Teisseyre, 1995 and references therein), so that the crack is popping out of the dislocation plane, but

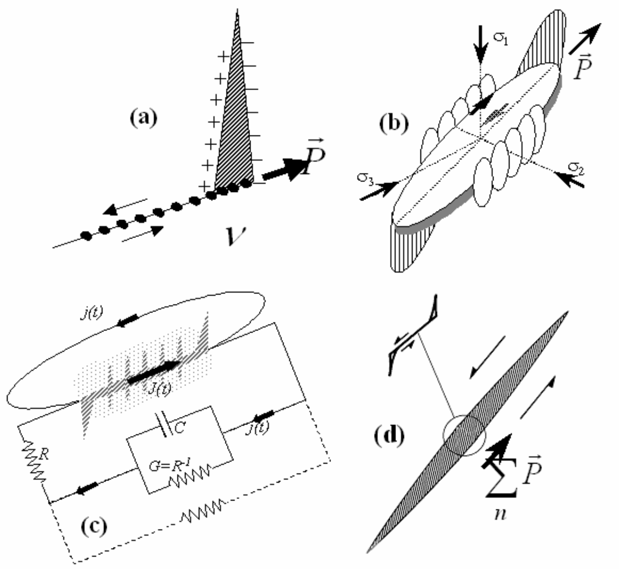

Fig. 1. (a) Sketch of a tensile (Mode I) crack forming at the tip of a dislocation array. The electric polarisation vector is the resultant of the polarisation vectors of ν dislocations, moving on the slip plane and sub-parallel to the slip vector. **(b)** 3-D schematic representation of a growing shear crack (adapted from Scholz, 1990). The polarisation vector is in the slip plane and parallel to the slip vector. **(c)** Side view of a propagating shear crack. The arrowed curve represents the conductive current destroying the polarisation fluctuations inside the crack. Current flow is simulated with an equivalent circuit comprising the shunt elements of a continuous distributed transmission line. Self-induction is negligible and the corresponding circuit element is not drawn. **(d)** Meso- and mega- scale cracks are ensembles of shear cracks with sub-parallel slip planes. The polarisation vector comprises the resultant of *n* simultaneously propagating microcracks.

opening up parallel to it. The shear stress causing the movement of the dislocation array is oriented in the slip plane of the array and, assuming a Griffith solid, it is inclined at an acute angle with respect to the compression axis σ_1. It is natural to assume that the crack field is the sum of the fields of the ν moving dislocations, oriented in the slip plane and perpendicular to the dislocation line. The movement of dislocations may form shear and transversal cracks, which are responsible for the ultimate failure of the rock. However, a shear crack cannot grow in its own plane, but only with the formation of axial tensile (Mode I) cracks at its tips (e.g. Nemat-Nasser and Horii, 1982; Teisseyre, 1995; Brace and Bombalakis, 1963). The upper and lower tips of the shear crack expand in a Mode II configuration, while its lateral edges are in Mode III and generate an array of Mode I axial cracks, as in Fig. 1b. The moving dislocations feed the tensile cracks by migrating (sub)parallel to the plane of the shear crack. Respectively, the resultant electric dipole moment is subparallel to the slip plane and in the direction of the slip vector. Eventually, the Mode I cracks at the lateral edges of the shear crack will reach a minimum critical distance with respect to each other and will begin to fuse. The array will be broken through by cracks parallel to the shear plane, forming a shear process zone as the first stage in forming a fault (Cox and Scholz, 1988).

Charge production and current generation during crack opening is a short-lived effect. Consider Fig. 1c, where the arrowed lines represent the current around an active shear crack, which can be simulated in terms of a transmission line

$$LC\frac{d^2 j(t)}{dt^2} + (RC + LG)\frac{dj(t)}{dt} + RGj(t) = j_0(t) \tag{2}$$

where all the material properties refer to the region outside the crack. The equation can be simplified assuming a quasi-homogeneous medium, in which case the ohmic properties of the shunt and series elements even out (RG=1). Furthermore, the second order term in Eq. (2) can be neglected because $(LC)^{1/2} \approx (\mu_0 \varepsilon_d l^2)^{1/2} = 10^{-11}$s, assuming an average dielectric constant $\varepsilon_d=10\varepsilon_0$ and distances l~10^{-3}m, of the order of the mean crack length. Likewise, when $\rho = 10^2$-10^6 Ωm, $LG \approx \mu_0 l\ (\rho l)^{-1} \approx 10^{-9}$-$10^{-14}$s and can also be neglected. Thus, Eq. (2) reduces to

$$RC\frac{dj(t)}{dt} + j(t) = J(t)\,, \tag{3}$$

with $j_0(t) \equiv J(t)$ the driving current, under the initial condition $J(t$=0)=0. The solution is:

$$j(t) = (RC)^{-1}\, e^{\frac{t}{RC}} \int_0^t J(\tau)\, e^{\frac{\tau}{RC}}\, d\tau\,.$$

Now, consider that for common petrogenetic minerals and rocks with resistivities $\rho \in (10^6$-10^4 Ωm) and dielectric permitivities $\varepsilon_d \in (\varepsilon_0 - 80\varepsilon_0)$, $RC \approx \varepsilon_d\rho \approx 10^{-3}$-$10^{-8}$s, if no external sources are applied. This is comparable to the duration of crack opening t_c, of the order 10^{-4}-10^{-7}s for source dimensions 10^{-1}-10^{-4} m. Figure 2 shows $j(t)$ as a function of the crack propagation time t_c for two different crack time functions. In Fig. 2a (top), $J(t) \propto (\bar{d}/t_c)\exp(-t/t_c)$, observing a Brune source function with displacement $d(t)=(\bar{d}/t_c)(1-\exp(-t/t_c))$. In Fig. 2b(top) the source function is $J(t) \propto \bar{d}\cdot\gamma\cdot t_c^{-\gamma}\cdot t^{\gamma-1}\cdot\exp(-(t/t_c)^\gamma)$, i.e. a Weibull distribution with displacement $d(t)=\bar{d}\,(1-\exp(-t/t_c)^\gamma)$. In both cases, $j(t)$ follows the crack opening rate when the ratio RC/t_c is near unity. Differences appear when RC is too long or too short with respect to t_c. Since the dielectric constant ε_d cannot vary significantly, the differences should mainly be controlled by changes in resistivity. When the resistivity increases so that $RC > t_c$, (an unlikely case as it would exceed the values expected for crustal materials), the current delays up to a few times the duration of crack opening. When the resistivity decreases so that $RC < t_c$, (more likely in the real crust), the current attenuates faster than the crack propagation rate; charge production inside the crack is quickly destroyed and the electrical polarisation disappears almost as soon as the crack reaches its terminal size. Note that a similar problem has been treated by Molchanov and Hayakawa (1998), to whom the reader may refer for additional information.

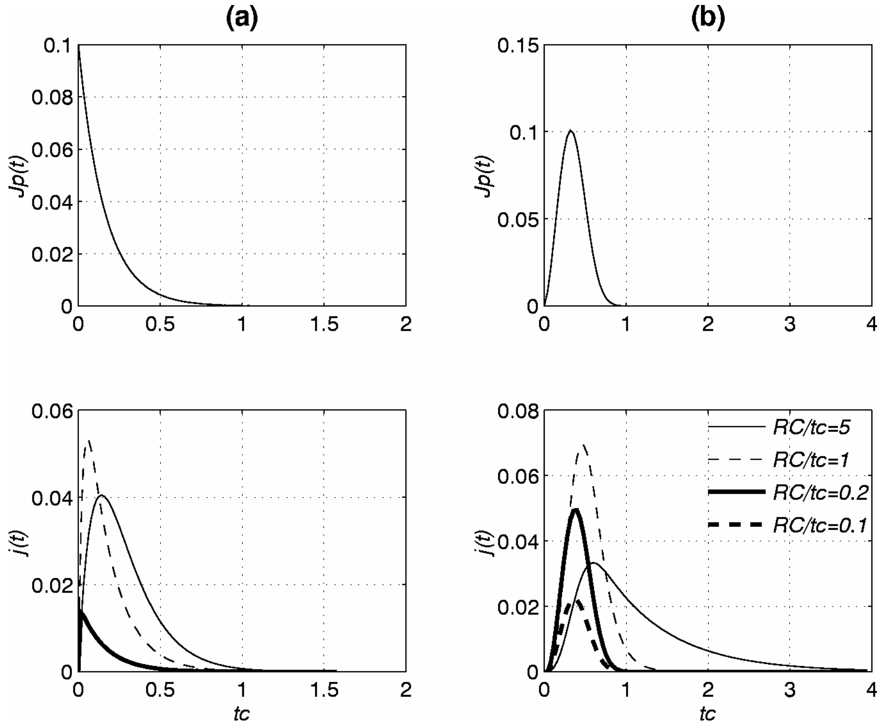

Fig. 2. Simulated current flow around a propagating shear crack for different crack time functions and different ratios RC/t_c.

2.1 The macroscopic electric field.

Meso- and mega-scale cracks and faults are fractal ensembles of micro- and meso-scale shear cracks propagating with sub-parallel slip planes subject to the same external shear stress, as is schematically depicted in Fig. 1d (see also Gueguen and Palciauskas, 1994; Scholz, 1990 and references therein). By the superposition principle, the electric dipole moment of meso- and macro-scale structures will comprise the resultant of all the simultaneously propagating microcracks, sub-parallel to the slip plane and in the general direction of the slip vector of the propagating fractures. At a point **r** and time *t*, the measured electric field may be qualitatively expressed as

$$\mathrm{E}(\mathbf{r},t) \approx c_s \sum_{i=1}^{\dot{n}(t)} (\rho J)_i \, \Gamma(\mathbf{r},\mathbf{r}_i) \cdot \left[\mathrm{u}(t) - \mathrm{u}\left(t - \frac{l_i}{\upsilon_i} \right) \right] \qquad (4)$$

where $\dot{n}(t)$ is the instantaneous number of active cracks, c_s is a sensitivity coefficient at the location of the receiver and $\Gamma(\mathbf{r}, \mathbf{r}_i)$ describes the propagation and attenuation of the dipole field generated by MCD and other effects due to the crack opening at point $\mathbf{r}_i$; u(t) is the Heaviside step function, l_i the crack propagation length and υ_i the opening velocity, so that the right hand factor in the sum allows the i^{th} crack to contribute only while it is opening.

A direct estimate of dislocation density under a wide range of conditions is given by $\delta\Lambda=\sigma/G$, where G is the shear modulus and σ is the applied shear stress (e.g. Turcotte and Schubert, 1982). By this definition, dislocation density varies dynamically during deformation, decreasing as the number and density of microcracks increases (also see Sornette and Sornette, 1990). Inasmuch as these quantities are practically indeterminable, it is rather infeasible to calculate estimates of the signal strength for real Earth materials. Laboratory experiments are the only real source of information in this respect. The dependence on resistivity is also a cardinal factor. If the dielectric constant remains the same and the resistivity decreases to, say, 100Ωm, charge redistribution will occur only after $RC \approx 10^{-9}$s. This is orders of magnitude faster than crack opening times and does not allow for a macroscopic field to build up as per Eq. (4), unless the number of cracks increases by a forbiddingly excessive factor. This is consistent with the majority of laboratory experiments, observing precursory electric signals in dry (resistive) samples. It also defines the limitation of the microfracturing / MCD concept, inasmuch as strong fields are expected only from resistive rock blocks.

2.2 A numerical simulation.

Let us, now, demonstrate that the superposition of many small, quasi parallel, simultaneous electric sources can be an efficient generator of macroscopic fields, observable faraway. We calculate the expected electric field, due to a fractally distributed set of emitters. Figure 3a illustrates a horizontal section of a simulated 'fault zone' with dimensions 5×1.5 km, comprising an ensemble of cells, each 50×15×50 m (=37500 m^3). The vertical dimension of the excited volume comprises a stack of 40 identical slices buried between 9-11 km. Microfracturing has percolated parallel to the long axis of the ensemble, representing the strike of the incipient fault which is located at a distance of 50km ENE of the observation point, in a half-space with resistivity of 100Ωm. Electrification in each cell is represented by a horizontal electric dipole of

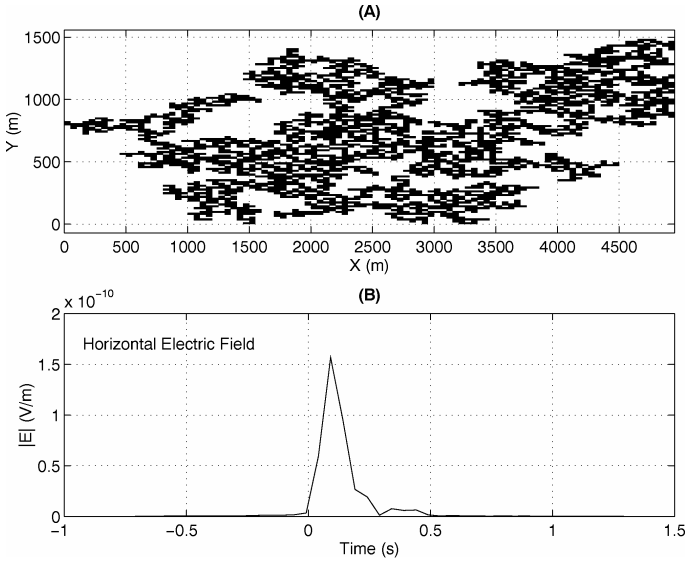

Fig. 3. (a) A horizontal slab model of a 'fault zone' comprising an ensemble of 100×100×40 cells, each with dimensions 50×15×50 m. Microfracturing has reached the percolation threshold, parallel to strike. **(b)** The transient variation of the horizontal electric field received at 50km WSW of the fault.

current moment 10^{-6} Am, located at its centre of gravity. We have adopted this value based on laboratory measurements of average currents from individual cracks (e.g. Warwick et al., 1982), assuming a mean crack length of $l_c=10^{-3}$m. We suppose that the cells do not emit in perfect unison, but with a small advance or delay with respect to each other, simulated with a random perturbation of the phase of each emitter (cell) sampled from the interval [-45°, 45°]. We also take the time constant of the electrification process to be of the order of $t_c=10^{-6}$s, i.e. comparable to the opening time of cracks with $l_c=10^{-3}$m: the entire ensemble emits quasi-instantaneously, with a short Dirac-δ time function. The field is calculated using the complete analytic solution of King et al., (1992, pp 155-159). Figure 3b shows the resulting transient variation of the horizontal electric field, with peak amplitude approx. 1.5×10^{-10} V/m. This result has been obtained by the superposition of approximately 1.2×10^5 individual dipoles, each representing a cell of 37500 m^3 in volume. It follows that it is sufficient to have one 10^{-6} Am dipole per m^3, to obtain a variation of 5.6 mV/km at a distance of 50 km from the focus. The plausibility and possibility of much stronger fields is therefore apparent, when the number of dipoles per m^3, or the resistivity of the source-receiver path increases by a mere order of magnitude.

2.3 Expected ledad times to earthquakes.

Crack propagation is inherent to brittle failure, while crack dynamics comprise the basis of all theories attempting to describe the processes leading to rupture. In earthquake seismology, the precipitous increase of crack production shortly prior to rupture is predicted by volume dilatancy models (e.g. Myachkin et al., 1975; Scholz, 1990), damage mechanics (e.g. Voight, 1989) and the critical point earthquake rupture model (e.g. Sornette and Sornette, 1990; Sornette and Sammis, 1995). The initiation and duration of crack propagation in large heterogeneous rock volumes depends on the mechanical and thermal history and the present state of the stressed materials, and may vary even between sub-regions of the same seismogenic volume. Nevertheless, all the theories and models of precursory phenomena indicate that stress and strain accumulation should become non-linear near the end of the loading cycle, producing greatly accelerated effects in the last one to several days prior to rupture (e.g. Stuart, 1988; Voight, 1989; Varnes, 1989; Scholz, 1990; Sornette and Sornette, 1990; Sornette and Sammis, 1995).

Figure 4 illustrates a qualitative sequence of events leading to the earthquake. Stage I is characterised by gradual increase in crack density with time and is not associated with electric phenomena, which are expected in Stage II, as the seismogenic volume enters a phase of massive crack propagation associated with high deformation rates – recall Eq. (1). By the end of this stage, crack interaction may cascade to rupture nucleation, or the system may remain in a critical state waiting for an additional event to tip the balance (Stage III). The temporary inhibition of rupture may result from factors such as are residual friction, dilatancy-hardening, stress reduction and last but not least, the heterogeneous distribution of stress, strain, crack density and material strength (for instance in asperities). The duration of Stage III is expected to vary according to the properties and conditions of the particular system, but it certainly cannot be long, given its extreme susceptibility to external factors. The generation of transient electric signals is inhibited during Stage III. Rupture follows in Stage IV, possibly but not necessarily accompanied by a co-seismic pulse, because at this point there's only a co-operative failure over different scales of already existing cracks. Note that Stages I-IV are generically associated with the corresponding Stages of the volume dilatancy models. As indicated previously, considerably accelerated deformation effects should be produced during the last several days (1-10) prior to the

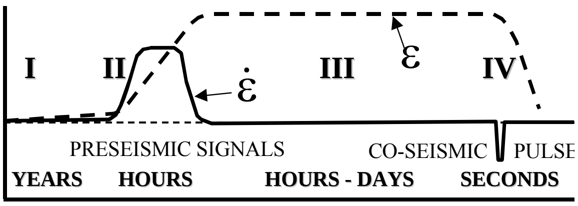

Fig. 4. Diagram in arbitrary time scale, depicting the evolution of deformation (broken line), and deformation rate (continuous line) prior to an earthquake.

earthquake; this defines the duration of Stages II-III and is consistent with observed time lags (Section 5).

3. Expected source time functions and signal waveforms

It is now accepted that brittle failure, (fracturing and fragmentation), is self-similar with respect to its geometry and critical point with respect to its dynamics (e.g. Sornette and Sornette, 1990; Turcotte, 1997 and references therein). It begins at the microscopic scale and cascades to the macroscopic by co-operative crack growth and coalescence in such a way, that fracturing at one scale (or level of the crack hierarchy), is part of damage accumulation at a larger scale. Once microfracturing begins, the number of propagating cracks (and the electric field) is first expected to rise sharply, but as the sustainable crack density is approached or stress/strain levels drop below a threshold value, it will decelerate and decline to zero when no more cracks can be produced. The duration of this process is unknown, but conceivably, it may require any time up to a few hours, depending on the size, mechanical and thermal state of the deforming volume. Tzanis et al. (2000) have constructed expressions for the time function of the EEP source, consistent with the phenomenology of brittle fracture as will be outlined forthwith.

The macroscopic behaviour of a large number of interacting cracks is, by nature, a problem of statistical mechanics and since cracks are organised in ensembles of distributed, interacting elements, it is appropriate to adopt a kinetic approach. This rather difficult problem has been taken up by a handful of authors (Petrov et al., 1970; Newman and Knopoff, 1983; Molchanov and Hayakawa, 1998) with varying degrees of success. We have found that by and large, the most complete and comprehensive treatment is in the theory of Czechowski (1991, 1995), which expands on assumptions similar to those of Boltzman's. The theory amounts to the kinetic equation

$$\frac{\partial f(\mathbf{x},l,t)}{\partial t}+\frac{\partial[\upsilon p f(\mathbf{x},l,t)]}{\partial l}= =\frac{1}{2}\int_0^l f(\mathbf{x},l_1,t)\,f(\mathbf{x},l-l_1,t)s\upsilon p\,\mathrm{d}l_1 - f(\mathbf{x},l,t)\int_0^\infty f(\mathbf{x},l_1,t)s\upsilon p\,\mathrm{d}l_1+N(l) \tag{5}$$

where $f(\mathbf{x},l,t)$ is a size distribution function of cracks such, that $f(\mathbf{x},l,t)\ \Delta\mathbf{x}\Delta l$ is the number of cracks which exist at time t within a volume element $\Delta\mathbf{x}$ around a point $\mathbf{x}$ and have sizes within Δl around size l,and where p is the probability and υ is the velocity with which cracks may propagate. The LHS of Eq. (5) expresses the changes in the number of cracks as resulting from the interactions described by the RHS. Specifically, the first term in the RHS is the total number of 'gains', i.e. the number of binary interactions whereby cracks with (smaller) sizes $l_1 < l$ collide and merge with cracks $l\text{-}l_1$ to produce cracks with sizes l, where $s=s(l,l_1,\overline{\sigma})$ is the cross section of collisions, $\overline{\sigma}$ is an average stress field and where the factor ½ prevents from counting an interaction twice. The second term in the RHS is the number of 'losses', i.e. the number of binary interactions whereby cracks of any size l_1 forming a beam with flux density $\mathrm{d}I=\upsilon p f(\mathbf{x},l,t)\mathrm{d}l_1$, collide with crack l and consume it. $N(l)$ is the nucleation term. The kinetic equation describes how cracks propagate and join each other with probability depending on the total cross-section of collisions between cracks. The quantities s, υ, and p may be functions of the size of cracks, stress field and properties of the rock. We are particularly interested in an analysis discretizing Eq. (5) in the size-space of cracks, according to

$$n_i(t)=\int_{L_{i-1}}^{L_i} f(l,t)\,\mathrm{d}\,l\,,$$

so that the total number of cracks is divided into m populations n_i, i=1,2,…,m with respect to their size. The case m=3 has been studied in Czechowski (1991). Successive integrations of Eq. (5) over the intervals $(0,L_1)$, (L_1,L_2), (L_2,∞), produce a set of 3 coupled ordinary differential equations,

$$\begin{aligned}\dot{n}_1 &= -(1-0.5k_1)n_1^2-n_1n_2-n_1n_3+\mathrm{n}_1\\ \dot{n}_2 &= 0.5(k_2-k_1)n_1^2-(1-0.5k_2)n_2^2-(1-k_2)n_1n_2-n_2n_3+\mathrm{n}_2\\ \dot{n}_3 &= 0.5(1-k_2)(n_1^2+2n_1n_2+n_2^3)-0.5n_3^2+\mathrm{n}_3\end{aligned} \tag{6}$$

where $\dot{n}_i=(\mathrm{s}_i\upsilon_i p_{i1})^{-1}\cdot(\mathrm{d}n_i/\mathrm{d}t)$. Equations (6) describe the balance of gains and losses of any given group of cracks by mergence (n_in_j denotes the fusion of cracks n_i with cracks n_j) and by propagation, where $\mathrm{n}_i=p_i(p_{i1}s_i)^{-1}\cdot[f(L_{i-1},t)-f(L_i,t)]$ is the propagation term. The factors k_j determine the span of interactions between any two crack populations, with $(1\text{-}k_j)$ representing the extent of losses due to healing. For a decreasing $f(l)$, $0<k_j<½$, with k_j=1/2 for $f(l)$ constant.

The case m=10 has been developed by Czechowski (1995), and utilised by Tzanis et al., (2000) and by us herein. Successive integrations of Eq. (5) over the intervals $(0,L_1]$, $(L_1,L_2]$, …, (L_9,∞) and subject to the constraints $0=L_0 < L_1 < \ldots < L_9 < L_{10} = \infty$ and L_i - L_{i-1} =1, produce a set of ten coupled ordinary differential equa-

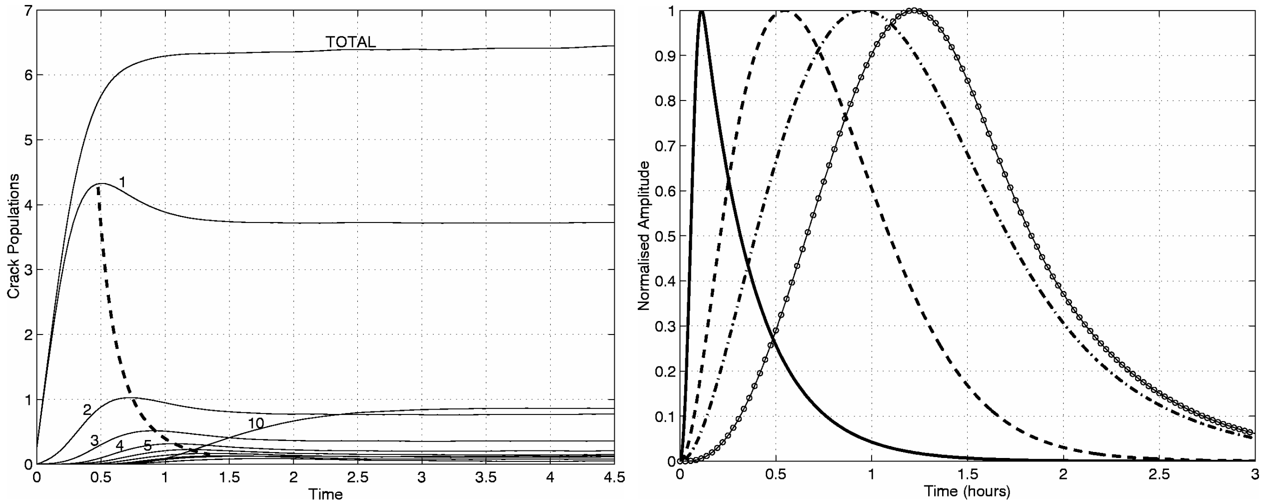

Fig. 5. (a) The evolution of ten crack populations with different sizes, following the kinetic theory of Czechowski, (1995). The numbers of cracks are given in relative units. (b) **N**ormalised time functions for different parameters of Eq. (9). Solid line, A=0.3×10^{-2}, β=2, α=-10^{-3}; dashed, A=0.2×10^{-3}, β=2, α=-10^{-3}; dash-dot, A=0.2×10^{-3}, β=2, α=5×10^{-4}; open circles, A=0.2×10^{-3}, β=3, α=5×10^{-3}. In all cases γ=1.

tions, similar in form to Eqs. (6). Using these, and assuming a constant production rate for the smallest crack population, in Fig. 5a we essentially reproduce the result of Czechowski (1995, figure 11.7.2a), but we also include the total number of cracks. The successive crack populations appear with a time delay following some power law (dashed line) such, that the total number of cracks behaves like a step function, asymptotically converging to a constant value as the crack density approaches saturation. This can be approximated by

$$n(t) = N_0(1 - \mathrm{e}^{-(\alpha t)^{\gamma}}) \tag{7}$$

Since only the propagating cracks are electric field sources, their time function should be

$$\dot{n}(t) = N_0 \gamma \alpha^{\gamma} t^{\gamma-1}\, \mathrm{e}^{-(\alpha t)^{\gamma}} \tag{8}$$

where α is a characteristic relaxation time and the exponent γ determines the shape. Equation (7) is in reality a Weibull cumulative distribution function and Eq. (8) the corresponding probability density function. Alternatively, an empirical description can be adopted, of the form

$$\dot{n}(t) = \mathrm{erf}\left([\mathrm{A}t]^{\beta}\right)\mathrm{e}^{-(\alpha t)^{\gamma}}\,\mathrm{u}(t) \tag{9}$$

where u(t) is the Heaviside step function with u(t)=1 for t>0 and u(t)=0 for t≤0. The constant A is a characteristic time of the crack production processes and β determines the slope of the rise time; both depend on material properties. It is instructive to consider a special cases of Eq. (9), appearing when γ=1, i.e. when the relaxation process is simple exponential decay. Using the series expansion for the error function, (Abramowitz and Stegun, 1972, p. 297),

$$\dot{n}(t) = \frac{2}{\sqrt{\pi}} \sum_{m=0}^{\infty} \frac{(-1)^m (\mathrm{A}t)^{\beta(2m+1)}\, \mathrm{e}^{-\alpha t}\mathrm{u}(t)}{m!(2m+1)}$$

If $\boldsymbol{F}$\{.\} is the Fourier transform operator, the frequency domain equivalent is

$$\begin{aligned}\dot{N}(\omega) = \boldsymbol{F}\{\dot{n}(t)\} &= \boldsymbol{F}\left\{\frac{2}{\sqrt{\pi}} \sum_{m=0}^{\infty} \frac{(-1)^m (\mathrm{A}t)^{\beta(2m+1)}\, \mathrm{e}^{-\alpha t}\mathrm{u}(t)}{m!(2m+1)}\right\} \\ &= \frac{2}{\sqrt{\pi}} \sum_{m=0}^{\infty} \frac{(-1)^m \mathrm{A}^{\beta(2m+1)}}{m!(2m+1)} \boldsymbol{F}\left\{ t^{\beta(2m+1)}\, \mathrm{e}^{-\alpha t}\mathrm{u}(t)\right\}\end{aligned}$$

The Fourier transform of the term in the brackets can be found in standard textbooks. We are interested in the case m=0, β(2m+1) >0.5, whereupon

$$\dot{N}(\omega) = \frac{2\mathrm{A}^{\beta}}{\sqrt{\pi}} \cdot \frac{\beta \cdot \Gamma(\beta)}{(\alpha + i\omega)^{\beta+1}}$$

featuring a corner frequency at α, spectral decay rate β+1 and a time domain transform

$$\dot{n}(t) = \frac{2}{\sqrt{\pi}} (\mathrm{A}t)^{\beta} \cdot \mathrm{e}^{-\alpha t}\mathrm{u}(t) \tag{10}$$

Equation (10) is an 'early time' version of Eq. (9), in the sense that the diverging first term of the error function expansion corresponds to some accelerating crack production, which would explode if it were not overcome by the exponential term. Examples of Eq. (9) for different parameters A, α and β are shown in Fig. 5b. These are characteristic shapes expected from the related family of functions (8)-(10). Variations of crack counts with a bell shaped envelope have often been seen prior to rupture, in recent experiments involving large rock samples (e.g.

Ponomarev et al., 1997; Feng and Seto, 1998, 1999; Baddari et al., 1999).

By virtue of Eq. (4), the received electric signal will be given by the convolution

$$\tilde{\mathrm{E}}(\mathbf{r},t) = \dot{n}(t) * \mathrm{E}(\mathbf{r},t) = c_s \dot{n}(t) * \sum_{i=1}^{\dot{n}(t)} (\rho J)_i \Gamma(\mathbf{r},\mathbf{r}_i) \cdot \left[\mathrm{u}(t) - \mathrm{u}\left(t - \frac{l_i}{\upsilon_i} \right) \right]$$

The duration of E(**r**, *t*) is of the order of a few to several seconds when t_c~10^{-7} -10^{-4} s. Moreover, frequencies higher than a few Hz do not propagate to intermediate or large distances from the source, (e.g. Vallianatos and Tzanis, 1998, 1999a). It is therefore expected that if $\dot{n}(t)$ is much slower than E(**r**, *t*), its waveform will predominate and determine the waveform of the resulting EEP. If the source time function is sufficiently slow, only the long periods of the resultant field $\tilde{\mathrm{E}}(\mathbf{r},t)$ are allowed to propagate.

4. Scaling Laws

If the microfracturing / MCD mechanism is indeed an EEP generator, a natural and spontaneous question is of whether EEP signal amplitudes scale by the magnitude of the impending earthquake. Given also the self-similarity of fragmentation processes, the question arises of how this scaling can be affected thereof.

There already exists such an empirical scaling law by Varotsos and Alexopoulos (1984), of the form log(ΔV)= bM + a, with b=0.3-0.4 and the intercept different for different seismic regions, earthquake sequences and source-receiver configurations. The quality of the data used to derive this law was seriously contested by many authors, (e.g. "Debate on VAN", Geophys. Res. Lett., 23(11), 1996; "A critical review of VAN", Lighthill, Sir J. (ed.), World Scientific, Singapore, 1996, etc.), but note that unless manipulated, it did allow the adequate determination of the parameters a and b. The authors attribute the almost universal slope to fundamental processes at the source, but cannot explain it. This was attempted by Sornette and Sornette (1990), on the basis of a critical point system, long range correlation between the earthquake source and the observer and piezoelectricity as the fundamental electrification process. Molchanov (1999) reproduced the relationship on the basis of electrokinetic effects, making the crucial assumption that the electric signal is a product of foreshock activity. Finally, Vallianatos and Tzanis (1999b) constructed a scaling law from first principles, only requiring that the source comprises a self-similar set of dipole emitters. Their result is consistent with dynamic microfracturing processes, as outlined in the following.

Consider an electrically polarised sphere of radius *L* and volume *V*, embedded in a conductive medium of constant resistivity ρ. Vallianatos and Tzanis (1999b) show that the observed horizontal electric field will be given by

$$\mathbf{E}_\mathrm{h}(t) = \frac{3V\rho}{4\pi R^3}\left(3\frac{\partial \mathrm{P}_z(t)}{\partial t}\cos\theta\sin\theta + \frac{\partial \mathrm{P}_1(t)}{\partial t}(3\sin^2\theta - 1)\right)\hat{\mathbf{e}}_\mathrm{h} = \frac{3V\rho}{4\pi R^3} K_{SR}(\theta,t)\hat{\mathbf{e}}_\mathrm{h} \tag{11}$$

where P_z is the vertical component of the polarisation, P_1 the horizontal component in source-receiver direction, *R* the hypocentral distance, θ the polar angle and $\hat{\mathbf{e}}_\mathrm{h}$ a horizontal unit vector along the epicentral radius at the location of observer.

Now, consider a spherical earthquake source volume V_s with radius L_s and a set of distributed spherical sub-volumes v_i with radii l_i in V_s, developing electrical polarisation, albeit not necessarily all at the same time (although only spherical sources are considered for the sake of simplicity, it is apparent that the theory may be generalised for sources with different shapes). This comprises a set of electrical emitters. Assuming that the number $\mathrm{N}(l_i)$ of sub-volumes with radius l_i, is distributed according to a power law of the form $\mathrm{N}(l_i) = A \cdot l_i^{-\mathrm{D}}$, $0<D<3$, by the fragmentation theory of Turcotte (1997), the total volume of the spherical emitters is given by

$$V_e = \sum_i v_\mathrm{i} = \frac{4\pi}{3}\frac{AD}{3-D}\left[l_{\max}^{3-D} - l_{\min}^{3-D} \right].$$

l_{max} is the uppermost radius size in v_i and a fraction κ of the maximum size L_s. l_{min} is the lowermost radius size and very likely comparable to the smallest crack size. Thus, we may assume $l_{min} << l_{max} \approx \kappa L_s$ and $0<<\kappa<1$, whereupon

$$V_e = \sum_i v_\mathrm{i} = \frac{4\pi}{3}\frac{AD}{3-D}(\kappa L_s)^{3-D} \tag{12}$$

The total observed horizontal electric field can be computed on the basis of the superposition principle. Inserting (12) into (11),

$$\mathbf{E}_h = \frac{3\rho}{4\pi R^3}\left(\sum_i v_i \right) K_{SR}\hat{\mathbf{e}}_\mathrm{h} = \frac{AD}{3-D}\rho K_{SR}\frac{(\kappa L_s)^{3-D}}{R^3} \tag{13}$$

The logarithm of Eq. (13) is

$$\log(\mathbf{E}_h) = (3-D)\log(L_s) + \log\left(\frac{AD\kappa^{3-D}}{3-D}\rho K_{SR} \right) - 3\log R \tag{14}$$

and by virtue of the well known scaling relationship $\log(L_s)$ = 0.5M + Const., (Scholz, 1990),

$$\log(\mathbf{E}_h) = \tfrac{1}{2}(3-D)\,\mathrm{M} + C_s \tag{15}$$

where C_s includes the second and third terms in the right hand side of Eq. (14).

A number of fragmentation experiments indicate that 2.2<*D*<2.8 (Turcotte, 1997) and the condition *D*>2 is nec-

necessary to render finite the total area of the fragments. Observations of fault networks indicate that the two-dimensional fractal dimension $D_2 \approx 1.6$, (Turcotte, 1997, p. 67), so that $D_3 = D_2 + 1 = 2.6$. Termonia and Meakin (1986) simulated the growth of two-dimensional cracks and found $D_2 = 1.27$, generalised as above to $D_3 = 2.27$, which is consistent with the experimental results quoted therein. Hirata et al. (1987) showed by means of experiment that $D_3 = 2.75$ for transient creep, $D_3 = 2.66$ for steady creep and $D_3 = 2.25$ for acceleration creep. The latter corresponds to the phase of dynamic crack propagation implying that as creep progresses, the crack network becomes increasingly clustered and the fractal dimension decreases. Thus, we may assume that D varies in the range (2.25-2.6), taking the lower values during dynamic crack propagation. Accordingly, the constant slope $\alpha = (3-D)/2$ varies in the range (0.375-0.2). In the presumed case of microfracturing, ($D \approx 2.3$), Eq. (15) becomes

$$\log(\mathbf{E}_h) = 0.35\,\mathrm{M} + C_s \qquad (16)$$

in which the slope 0.35 is very comparable to that of Varotsos and Alexopoulos (1984). We point out however, that the factor C_s is strongly dependent on the source and source-receiver path (second term in Eq. 14), but only weakly on the source-receiver separation (third term), because the product $3\log R$ changes slowly. Therefore, any empirical realisation of Eq. (16) at a given location, *cannot* be used as a universal standard to predict the magnitude of the impending earthquake at another place.

5. Examples

5.1 A possible EEP to the 17 January 1983, M7 Kefallinia earthquake (Ionian Sea).

This was one of the largest events to have occurred at the Ionian Sea in the 20th century, with its epicentre located SW of Kefallinia island, (ISC co-ordinates 38.09°N, 20.19°E), at a focal depth of 9 km. In spite of the many research papers it generated, the focal mechanism is still unclear. A dextral strike-slip mechanism on a NE-SW plane parallel to the Kefallinia Transform is favoured by several authors, while a thrust fault on a NW-SE plane is preferred by others (see Baker et al., 1997, for a thorough review). The Harvard CMT solution used herein indicates rupture compatible with NE-SW compression, either a steep thrust on a NW-SE plane with azimuth 151°, dip 84°, rake 77° and slip vector oriented at 124° and dipping at 76°, or a very shallow oblique slip thrust on a NE-SW plane, with azimuth 34°, dip 14°, rake 154° and slip vector oriented at 241° and dipping at 6° (Fig. 7).

Varotsos and Alexopoulos (1984) claim to have recorded an electrical precursor to this earthquake at their PIR station, approximately 130 km SE of the epicentre, (Fig. 7), which they illustrate in figure 7 of *their* paper. It comprises a bay-like, long period waveform beginning on approx. 14:00 of 15 January 1983, superimposed on a non-linear variation of the background. We have reproduced a digital version by scanning *their* figure at high resolution and digitising it on a computer monitor (Fig.

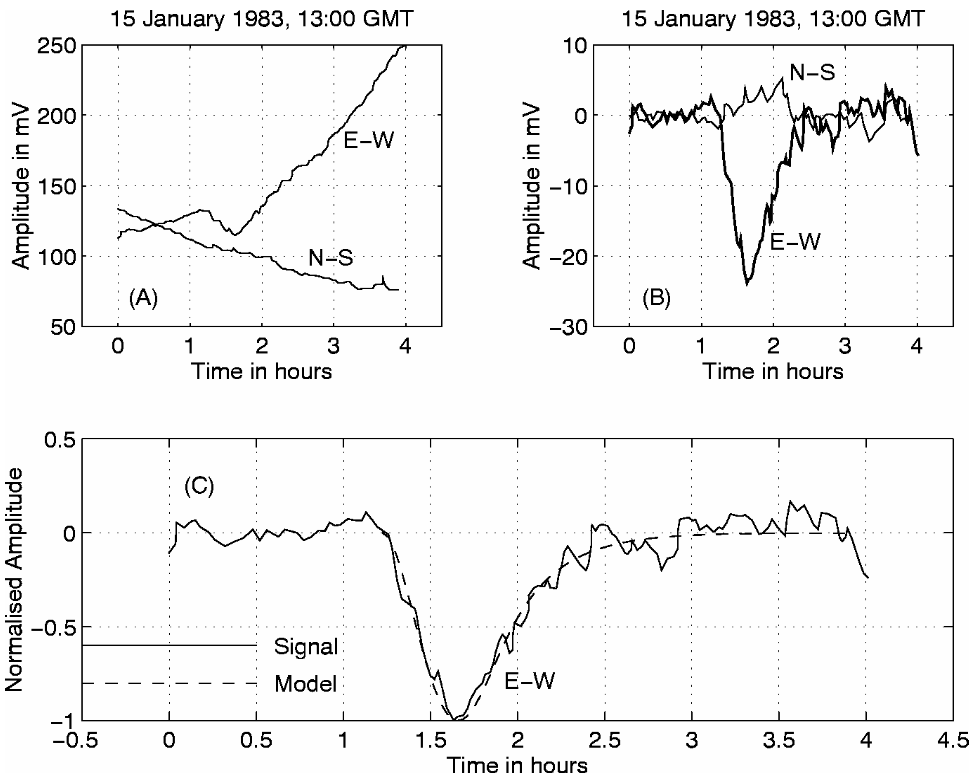

Fig. 6. (a) The digitised signal recorded by Varotsos and Alexopoulos (1984a) on 14:00 GMT of 15 January 1983 at Pyrgos, Greece, and reported as precursor to the 17 January 1983 Kefallinia earthquake. (b) The same signal after removing the background. Hour 0 corresponds to 13:00 GMT. (c) A model of the normalised E-W component using Eq. (9).

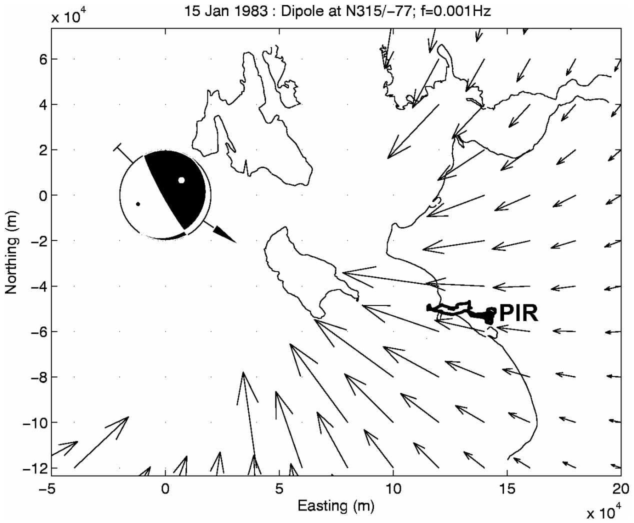

Fig. 7. The horizontal vector field at 0.001Hz, due to an electric dipole, buried at the ISC hypocentre of the 17/01/1983 Kefallinia earthquake. The dipole's horizontal projection is indicated by the T-bar and its positive pole is oriented at N315°/-77° (head of the 'T-bar'). The polarisation of the observed signal (thick line at PIR), the Harvard CMT focal mechanism and the horizontal projection of the slip vector corresponding to the NW-SE nodal plane (arrow), are also shown.

6a). On removing the background, we obtain a strong E-W component (25mV/50m), but very weak N-S (Fig. 6b). The E-W waveform is asymmetric, with faster rise time, slower exponential-like decay and total duration no longer than 2 hours. The main part of the signal stands clearly above noise, the peak amplitude of which is approximately 20% of the peak signal amplitude. The later times however, are obscured and it is rather difficult to assess the exact waveform and duration of the decay phase.

The shape of the long period E-W components can be easily fitted with functions of the form (8)-(10). In Fig. 6c we present a model based on Eq. (9), with $\gamma=1$ and $A\approx5.3\times10^{-4}$, $\beta\approx2.1$, $\alpha\approx9.9\times10^{-4}$. Note that $2\pi/\alpha\approx6300$s (1.75 hours), is approximately the duration of the model, $1/\alpha$ is a characteristic relaxation time and $\alpha/2\pi$ is the corner frequency. In Fig. 7, we illustrate the horizontal vector field of a unit electric dipole at the frequency of 0.001Hz, buried at d=10000m in a half-space of conductivity 0.01S/m and oriented at N315°/-77°. The horizontal projection of the dipole is indicated with the 'T-bar'. In the vicinity of PIR, this configuration generates, a predominantly E-W horizontal vector field, with polarisation very similar that of the observed signal, also shown for comparison. The direction N315°/-77° compares very well with the direction of the slip vector of the first nodal plane of the Harvard CMT solution, (N124°/76° - arrow in Fig. 7), but indicates an opposite polarity, in the sense that the positive pole of the dipole is oriented parallel and opposite to the direction of the slip vector. Figure 7 shows the optimal member of a family of similar dipole configurations generating similar results. This is consistent with the postulation that MCD electrification occurs parallel to the slip vector of dislocations, cracks, fractures and faults.

The 15 January 1983 signal recorded by Varotsos and Alexopoulos (1984) realises all the predictions of the microfracturing / MCD model. It appeared only at the terminal phase of the earthquake cycle (2.5 days prior to the main shock), with time dependence as expected by the crack propagation model, and polarisation characteristics reproducible under the assumption of electrification parallel to the slip vector of the impending earthquake. The latter is consistent with the focal mechanism solutions favouring a NW-SE thrust fault. Buried dipoles at directions consistent with the slip vector of the NE-SW plane *cannot* reproduce the observed polarisation. Moreover, this signal was the first of a series distributed according to an amplitude-magnitude scaling law consistent with our theoretical prediction of Section 5; there's a strong possibility that it might have been generated by a set of emitters with fractal dimension of approx. 2.3, which is hard to be explained in terms of anthropogenic noise.

A critical approach to the above results may point out the absence of any direct proof of the seismic origin of the signal and argue that the difficulties of reconstructing the signal properties are serious and insurmountable, thus rejecting them as purely coincidental. It may also be pointed out that it is premature (if not impermissible) to discuss about constraining earthquake focal mechanisms with precursory electrical data of 'uncertain' nature. We cannot assign the probability that our modelling results are coincidental, but we can argue that the compliance of the signal with a generic model of the earthquake source renders its seismic origin quite possible, at least until the model can be refuted. The answer to either point of view will remain unknown, until a large amount of well constrained data is accumulated and EEP generation models are developed to sufficient detail.

5.2 A possible EEP to the 18 November 1992, M5.9 Galaxidi Earthquake (Gulf of Corinth, Central Greece).

The event with M_S=5.9 occurred offshore at 38.30°N, 22.43°E (ISC) with a focal depth of 7-10 km. The focal mechanism solutions by Harvard (CMT), Briole et al. (1993) and Karakaisis et al. (1993), are all remarkably similar and indicate either a low angle E-W normal fault dipping N, or a somewhat steeper E-W normal fault dipping S. According to Karakaisis et al. (1993), the mean parameters of the north dipping plane are azimuth 258°, dip 31°, rake -81°, with slip vector azimuth 340° and dip -31°, while the mean parameters of the S-dipping plane are azimuth 68°, dip 60°, rake -95° and slip vector azimuth 170° and dip -59, (see Fig. 9). Hatzfeld et al., (1996) identified the low angle N-dipping plane to be the fault, but Briole et al. (1993) discuss both cases and conclude that the earthquake occurred on the S-dipping normal fault.

In hindsight, we can recognise several phenomena that may be interpreted as precursory to this earthquake. According to Tselentis and Ifantis (1996), a large number of very small earthquakes (M<2), were recorded at the station NAF of the local permanent network of the Univer-

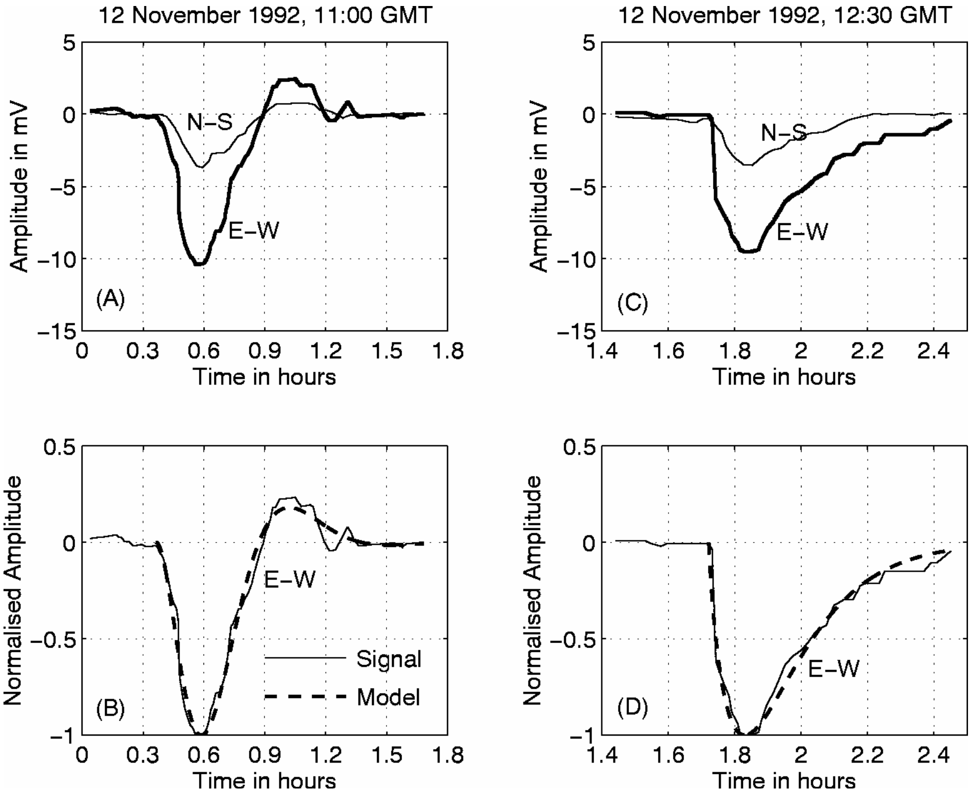

Fig. 8. (a) The first signal recorded by Tselentis and Ifantis (1996) on 11:20 GMT of 12/11/1992 at Patras, Greece, and reported as precursor to the 18/11/1992 Galaxidi earthquake. Hour 0 corresponds to 11:00 GMT. (b) A model of the normalised long period E-W component constructed with Eq. (17). (c) The second signal of Tselentis and Ifantis (1996), with arrival at 12:40 GMT of 12/11/1992. The time axis is annotated relative to that of Fig. 8a. (d) A model of the normalised E-W component constructed with Eq. (10).

sity of Patras (see Fig. 9), as of 11-11-1992. These events reached a peak rate of several hundreds per day. We did not find any other published account of this phenomenon. Abbad, (1993) reports a strong radon emission anomaly, which started building up by the late hours of 12 November at station KAL (Fig. 9), approximately 20km to the NW of the epicentre and culminated the next day. These observations are *direct* evidence of microfracturing, given that radon is released from the host rock by such a process.

A transient electric variation was observed on 12 November 1992, at the University of Patras Campus, approximately 70 km west of the epicentre (Fig 9). Tselentis and Ifantis report this signal as EEP, (1996, in *their* figure 10), but do not make any attempt to identify and authenticate it, appearing content with the fact that "no other anomaly of the geoelectric field was recorded prior to the event". The published signal was sufficiently clear and annotated, as to warrant digital reproduction. It comprises, two distinct waveforms with identical polarisation. The first arrived just after 11:20 GMT. It had peak-to-peak amplitude 12.3 mV, lasted for a little more than one hour and resembled a damped sinusoid (Fig. 8a). The second arrived just after 12:40 GMT, had a peak amplitude of 9.5 mV, lasted for almost one hour and had an asymmetric bell shape.(Fig. 8c). In spite of the different waveforms, the identical polarisation of the two signals points toward common, or at least proximate source regions.

The first signal cannot be modelled exactly, with equations (8)-(10). In keeping the discussion simple, we introduce the function

$$\dot{n}(t) = t^{\beta} \cdot \sin(\xi t) \cdot \mathrm{e}^{-\alpha t} \mathrm{u}(t) \tag{17}$$

describing a linear system with feedback proportional to the derivative of its output (see Rohrs et al., 1993). Such a system could possibly describe crack propagation, if stress is the input depending on a set of past state variables, and strain rate the output. This system would be self-regulating, with its state continuously varying with time. It may be that Eq. (17) represents a more general case, with Eqs. (8)-(10) being time functions of simpler (and possibly more common) processes without this type of feedback. This hypothesis cannot be tested because we know of only this example and we do not know under which conditions the system (17) would be realisable. The signal may be fitted with the parameters α=0.001772, β=1.25, ξ= 0.001728 and the model is shown in Fig. 8b. Note that the sinusoidal modulator frequency (ξ) is comparable to the characteristic time (α) of the signal, indicating the time constant of the hypothesised feedback mechanism. The second signal may be better modelled with Eq. (10) and parameters α=0.00203 and β=0.84

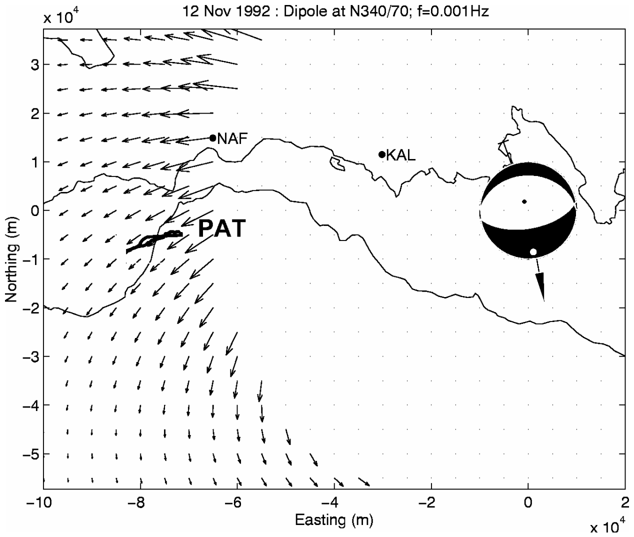

Fig. 9. The horizontal vector field at 0.001Hz, due to an electric dipole located at the ISC hypocentre of the 18/11/1992 Galaxidi earthquake. Its horizontal projection is indicated by the T-bar and its positive pole is oriented at N340°/70° (head of the 'T-bar'). The polarisation of the observed signal (thick line at PAT), the focal mechanism of Karakaisis et al., (1993) and the horizontal projection of the slip vector of the S-dipping nodal plane, (arrow), are also shown.

($2\pi/\alpha \approx 3100$ s, is again comparable to its duration, Fig. 8d).

In Fig. 9, we illustrate the horizontal vector field of a unit electric dipole at the frequency of 0.001Hz, buried at d=10000m in a half-space of conductivity 0.01S/m and oriented at N340°/70°. The configuration of the electric dipole is consistent with the slip vector of the second nodal plane in the focal solutions of Briole et al., (1993) and Karakaisis et al., (1993). The inclination of the dipole must be steeper than the slip vector by 10°, but is still consistent with the solutions. In this case as well, the direction of the electric dipole is oriented opposite to the sense of slip. In this case, the electrical precursor appears to favour the case of a steep south dipping normal fault, but the same reservations and comments apply, as per Subsection 5.1.

6. Conclusions

The spontaneous generation of transient electric current during the fracturing of non-piezoelectric rock samples has long been observed by experiment, but the underlying mechanism(s) have not been clarified. Our work expands on the hypothesis that the main source of this current may be the motion of charged edge dislocations during crack formation and propagation, which is expected at the terminal phase of the earthquake cycle. Other mechanisms are not excluded, but are rather considered to accompany and supplement the drastic MCD process. The basic idea is that an observable macroscopic ULF field can be generated by the superposition of multiple simultaneous tiny sources, not large and implausibly powerful current elements.

In theory, such a process is feasible and efficient, albeit only in unsaturated or dry rocks, and is thought to generate an electric dipole field in the general direction of the slip vector of the incipient fault. We present two examples of signals observed prior to earthquakes (out of several), in which the polarisation of the electric field matches with the polarisation expected from electric dipoles associated with the slip vector of a particular nodal plane and focal mechanism solution, out of several alternatives. Moreover, it appears possible to model the evolution of large crack ensembles and derive the expected time functions of transient EEP events. We have concluded to a family of bell shaped time functions and successfully applied them to model the shape of the example signals. Finally, we have shown from first principles that in the case of dynamic crack propagation associated with electrification, the precursory signal amplitude and earthquake magnitude are related with a self-similar law of the form $\log\mathbf{E}=C_s+bM$, where $b\approx0.35$ and C_s depends on the source properties and source-receiver path; such a law has been empirically constructed from experimental data by Varotsos and Alexopoulos (1984).

The model makes specific predictions about the properties of a certain class of transient electric precursors, but while it is plausible and testable, it is still incomplete, requiring further development and verification. An additional difficulty is that well constrained EEP signals such as presented in Section 5 are relatively rare in the literature, inasmuch as it is no always possible to have observable electric signals during crack propagation. It is clear that a great deal of work is needed, before one can claim a working theory of the earthquake preparation process but it is also apparent that that observed signals can indeed be described with generic theories of the source.

Acknowledgements: The work of one of the authors (F.V.) was supported by grant INTAS 99-1102

References

Abbad, S., *Etude des variations de l'activite volumique radon en fonction des parametres meteorologiques et geologiques*. Thesis, University of Paris VII, 1993 (in French).

Abramowitz, M. and I.A. Stegun, *Handbook of Mathematical Functions*, Dover, New York, 1972

Baddari. K., G.A. Sobolev, A. Frolov, and A. Ponomarev, An integrated study of physical precursors of failure in relation to earthquake prediction, using large scale rock blocks, *Annali di Geofisica*, **42**, 771-787, 1999.

Baker, C., D. Hatzfeld, H. Lyon-Caen, E. Papadimitriou, and A. Rigo. Earthquake mechanisms of the Adriatic sea and western Greece : implications for the oceanic subduction - continental collision transition, *Geophys. J. Int.*, **131**, 559-594, 1997.

Bella, F., P.F., Biagi, M. Caputo, G. Della Monica, A. Ermini, W. Plastino, and V. Sgrigna, Electromagnetic background and preseismic anomalies recorded in the Amare cave, (central Italy), in *Electromagnetic Phenomena Related to Earthquake Prediction*, ed. by M. Hayakawa and Y. Fujinawa, pp. 181-192, TERRAPUB, Tokyo, 1994.

Brace, W.F. and Bombalakis, E.G., A note on brittle crack growth in compression, *J. Geophys. Res.*, **68**, 3709-3713, 1963.

Briole, P., A. Deschamps, H. Lyon-Caen, K. Papazissi and J. Martinod. The Itea (M_S ~ 5.9) earthquake of November 18, 1992, Characteristics of the main shock inferred from body wave and ground displacement analysis. *Proceedings, 2nd Congress of the*

Hellenic Geophysical Union, Florina, Greece, 5-7 May 1993, Vol. **1**, 297-308, 1993.

Chen, D., D. Zhang and Z. Sun. ULF electric potential changes prior to fracture in rock samples, in *Electromagnetic Phenomena Related to Earthquake Prediction,* ed. by M. Hayakawa and Y. Fujinawa, pp. 323-329, TERRAPUB, Tokyo, 1994.

Cress, G.O., B.T. Brady and G.A. Rowell, Sources of electromagnetic radiation from fracture of rock samples in laboratory, *Geophys. Res. Lett.,* **14**, 331-334, 1987.

Czechowski, Z., A kinetic model of crack fusion, *Geophys. J. Int.,* **104**, 419-422, 1991.

Czechowski, Z., Dynamics of fracturing and cracks, in *Theory of Earthquake premonitory and fracture processes*, ed. by R. Teisseyre, pp. 447-469, Polish Scientific Publishers, 1995.

Cox, S.J.D. and C.H. Scholz, On the formation and growth of faults: An experimental study, *J. Struct. Geol.,* **10**, 413-430, 1988.

Enomoto, J. and H. Hashimoto, Emission of charged particles from indentation fracture of rocks, *Nature,* **346**, 641-643, 1990.

Enomoto, Y., T. Shimamoto, A. Tsutsumi and H. Hashimoto, Transient electric signals prior to rock fracturring: Potential use as an immediate earthquake precursor, in *Electromagnetic Phenomena Related to Earthquake Prediction*, ed. by M. Hayakawa and Y. Fujinawa, pp. 253-259, TERRAPUB, Tokyo, 1994.

Ernst, T., J. Jankowski, C. Rozluski and R. Tesseyire, Analysis of the electromagnetic field recorded in the Friuli seismic zone, NE Italy, *Tectonophysics,* **224**, 141-148, 1993.

Eshelby, J.D., F.C. Frank and F.R.N. Nabarro, The equilibrium of linear arrays of dislocations, *Philos. Mag.,* **42**, 351-364, 1951.

Feng, X-T and M. Seto, Neural network dynamic modelling of rock microfracturing sequences under triaxial compressive stress conditions, *Tectonophysics*, **292**, 293-309, 1998.

Feng, X-T and M. Seto, Fractal structure of the time distribution of microfracturing in rocks, *Geophys. J. Int.*, **136**, 275-285, 1999.

Fiffolt, D.A., V.F. Petrenko and E.M. Schulson, Preliminary study of electromagnetic emissions from cracks in ice, *Philos. Mag.* **B67**, 289-299, 1993.

Freund, F. and J.G. Borucki. Charge carrier generation and charge cloud propagation following 100m/sec impacts on igneous rocks, in *Atmospheric and Ionospheric Electromagnetic Phenomena Associated with Earthquakes*, ed. by M. Hayakawa , pp. 839-857, TERRAPUB, Tokyo, 1999.

Gueguen, Y. and V. Palciauskas, *Introduction to the physics of rocks*, Princeton University Press, Princeton, 1994.

Hadjicontis, V. and C. Mavromatou, Transient electric signals prior to rock failure under uniaxial compression, *Geophys. Res. Lett.,* **21**, 1687-1690, 1994.

Hadjicontis, V. and C. Mavromatou, Laboratory investigation of electric signals preceding earthquakes, in *A critical review of VAN*, ed. by Sir J. Lighthill, pp. 105-117, World Scientific, Singapore, 1996.

Hatzfeld, D., D. Kementzetzidou, V. Karakostas, M. Ziazia, D. Nothard, D. Diagourtas, A. Deschamps, G. Karakaisis, P. Papadimitriou, M. Scordilis, R. Smith, N. Voulgaris, A. Kiratzi, K. Makropoulos, M-P. Bouin and P. Bernard, The Galaxidi Earthquake of 18 November 1992 : A Possible Asperity within the Normal Fault System of the Gulf of Corinth (Greece). *Bull. Seismological. Soc. Am.,* **86**, 1987-1991, 1996.

Hirata, T., T. Satoh and K. Ito, Fractal structure of spatial distribution of microfracturing in rock, *Geophys. J. R. Astr. Soc.,* **107**, 155-162, 1987.

Karakaisis, G., B. Karakostas, E. Scordilis, A. Kiratzi, D. Diagourtas, P. Papadimitriou, N. Voulgaris and M. Ziazia, The spatial properties of the aftershocks and the focal mechanism of the Galaxidi earthquake (central Greece) of November 18, 1992. *Proceedings, 2nd Congress of the Hellenic Geophysical Union,* Florina, Greece, 5-7 May 1993, vol. **1**, 309-317, 1993.

King, R.W.P., M. Owens and T.S. Wu, *Lateral Electromagnetic Waves*, Springer Verlag, 1992.

Molchanov, O.V. and M. Hayakawa, On the generation mechanism of ULF seismogenic electromagnetic emissions, *Phys. Earth Planet. Int.*, **105**, 201-210, 1998.

Molchanov, O.V., Fracturing as underlying mechanism of seismoelectric signals, in *Atmospheric and Ionospheric electromagnetic phenomena associated with Earthquakes,* ed. by M. Hayakawa, pp. 349-356, TERRAPUB, Tokyo, 1999.

Myachkin, V., W. Brace, G. Sobolev and J. Dieterich, Two models of earthquake forerunners, *Pure Appl. Geophys.,* **113**, 169-181, 1975.

Nemat-Nasser, S. and H. Horii, Compression-induced nonplanar crack extension with application to splitting, *J. Geophys. Res.,* **87**, 6805-6821, 1982.

Newman, W.I. and L. Knopoff, Crack fusion as a model of repetitive seismicity, *Pure Appl. Geophys.* **121**, 495-510, 1983.

Nitsan, U., Electromagnetic emission accompanying fracture of quartz-bearing rocks, *Geophys. Res. Lett.,* **4**, 333-337, 1977.

Nomikos, K. and F. Vallianatos, Transient electric variations associated with large intermediate-depth earthquakes in South Aegean, *Tectonophysics,* **269**, 171-177, 1997.

Ogawa, T., K. Oike and T. Miura, Electromagnetic radiation from rocks, *J. Geophys. Res.,* **90**, 6245-6249, 1985.

Petrov, V.A., V.I. Vladimirov and A.N. Orlov, A kinetic approach to fracture of solids - I. General theory, *Phys. Stat. Sol.,* **42**, 197-206, 1970.

Ponomarev, A.V., A.D. Zavyalov, V.B. Smirnov and D.A. Lockner, Physical modelling of the formation and evolution of seismically active fault zones, *Tectonophysics*, **277**, 57-81, 1997.

Rohrs, C.E., J.L. Melsa and D.G. Schultz, *Linear control systems*, McGraw Hill, 1993.

Scholz, C.H., *The Mechanics of Earthquakes and Faulting*, Cambridge University Press, 1990.

Slifkin, L., Seismic electric signals from displacement of charged dislocations, *Tectonophysics,* **224**, 149-152, 1993.

Sornette, A. and D. Sornette, Earthquake rupture as a critical point: consequences for telluric precursors, *Tectonophysics,* **179**, 327-334, 1990.

Sornette, D. and C.G. Sammis, Complex critical exponents from renormalization group theory of earthquakes: Implications for earthquake predictions, *J. Phys. 1*, **5**, 607-619, 1995.

Stroh, A.N., The formation of cracks as a result of plastic flow, *Proc. R. Soc. London, Ser. A,* **223**, 404-414, 1954.

Stuart, W.D., Forecast model for great earthquakes at the Nankai trough subduction zone. *Pure Appl. Geophys.,* **126**, 619-641, 1988.

Teisseyre, R., Dislocations to crack processes, in *Theory of Earthquake premonitory and fracture processes*, ed. by Teisseyre, R., pp. 237-245, Polish Scientific Publishers, 1995.

Teisseyre, R. and H. Nagahama, Dislocational models of electric field generation in a seismic source zone, *Atmospheric and Ionospheric Electromagnetic Phenomena Associated with Earthquakes*, ed. by in M. Hayakawa, pp. 271-285, TERRAPUB, Tokyo, 1999.

Termonia, Y. and P. Meakin, Formation of fractal cracks in a kinetic fracture model, *Nature*, **320**, 429-431, 1986.

Tselentis, G-A and A. Ifantis, Geoelectric variations related to earthquakes observed during a 3-year independent investigation, *Geophys. Res. Lett., Special Issue 'Debate on VAN',* **23**, 1445-1448, 1996.

Turcotte, D.L., *Fractals and chaos in geology and geophysics*, Cambridge University Press, 1997.

Turcotte, D.L. and G. Schubert, *Geodynamics. Applications of Continuum Physics to Geological Problems*, Willey, New York, 1982.

Tzanis, A., F. Vallianatos and S. Gruszow, Identification and discrimination of transient electrical earthquake precursors: Fact, fiction and some possibilities, *Phys. Earth. Planet. Int.,* **121,** 223-248, 2000.

Vallianatos, F. and A. Tzanis. Electric current generation associated with the deformation rate of a solid : Preseismic and coseismic signals, *Phys. Chem. Earth*, **23**, 933-938, 1998.

Vallianatos, F. and A. Tzanis. A model for the generation of precursory electric and magnetic fields associated with the deformation rate of the earthquake focus, in *Atmospheric and Ionospheric* *electromagnetic phenomena associated with Earthquakes,* ed. by M. Hayakawa , pp. 287-305 TERRAPUB, Tokyo, 1999a.

Vallianatos, F. and A. Tzanis. On possible scaling laws between Electric Earthquake Precursors (EEP) and Earthquake Magnitude, *Geophys. Res. Lett*., **26** (13), 2013-2016, 1999b.

Varnes, D.J., Predicting earthquakes by analysing accelerating precursory seismic activity, *PAGEOPH*, **130**, 661-686, 1989.

Varotsos, P. and K. Alexopoulos, Physical properties of the variations of the electric field of the earth preceding earthquakes, I, *Tectonophysics,* **110**, 73-98, 1984.

Voight, B., A relation to describe rate-dependent material failure, *Science*, **243**, 200-203, 1989.

Warwick, J.W., C. Stoker and T.R. Meyer, Radio emission associated with rock fracture : Possible application to the great Chilean earthquake of May 22, 1960, *J. Geophys. Res.*, **87**, 2851-2859, 1982.

Whitworth, R.W., Charged dislocations in ionic crystals, *Advances in Physics,* **24**, 203-304, 1975

Yoshida, S., P. Manjgaladze, D. Zilpimiani, M. Ohnaka and M. Nakatani. Electromagnetic emissions associated with frictional sliding of rock, in *Electromagnetic Phenomena Related to Earthquake Prediction*, ed. by M. Hayakawa and Y. Fujinawa, pp. 307-322, TERRAPUB, Tokyo, 1994.

Yoshida, S., M. Uyeshima and M. Nakatani. Electric potential changes associated with a slip failure of granite : Preseismic and coseismic signals, *J. Geophys. Res.*, **102**, 14883-14897, 1997.

Andreas Tzanis and Filippos Vallianatos (e-mail fvallian@chania.teiher.gr)